Powder Technology 452 (2025) 120561

Contents lists available at ScienceDirect

Powder Technology

journal homepage: www.journals.elsevier.com/powder-technology

The purification of mesoscopic graphene flakes via eddy current separation

Cao Bin [a,b,c,e,1], Yuan Yi [a,1], Shan Zhicheng [a,b], Yang Lixue [a], Ali Reza Kamali [a,d,*], Wang Qiang [b,**], Diogo Montalvão [c,**], Amor Abdelkader [c,**]

[a] School of Metallurgy, Northeastern University, Shenyang 110819, China
[b] Key Laboratory of Electromagnetic Processing of Materials (Ministry of Education), Northeastern University, Shenyang 110819, China
[c] Department of Design and Engineering, Faculty of Science & Technology, Bournemouth University, Poole, Dorset BH12 5BB, United Kingdom
[d] Energy and Environmental Materials Research Center (E^2MC), Northeastern University, Shenyang 110819, China
[e] Ganjiang Innovation Academy, Chinese Academy of Sciences, Ganzhou 341119, China

HIGHLIGHTS

- A new physical purification method for graphene has been proposed;
- Eddy current separation shows promise for purifying mesoscopic graphene;
- Electrodynamic force on high aspect ratio graphene in a magnetic field computed;
- Graphene flakes with fewer layers exhibit higher settling terminal velocities.

GRAPHICAL ABSTRACT

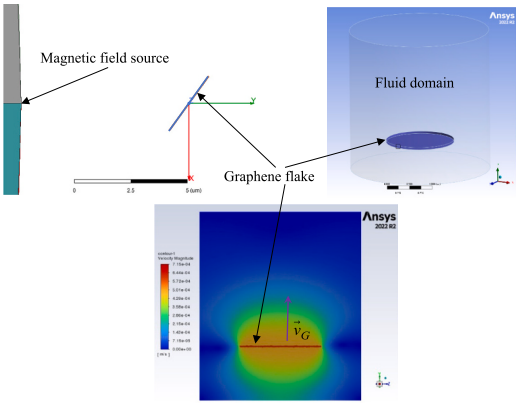

ARTICLE INFO

Keywords:
Graphene
Eddy current separation
Purification process
Numerical simulation

ABSTRACT

The exceptional properties of graphene are highly sensitive to impurities, which restrict its applications. Nearly all large-scale production methods fall short of adequately controlling impurities introduced during manufacturing. Given the significant differences in electrical conductivity between graphene and non-graphene impurities, we explore the application of eddy current separation for the purification of graphene. Through numerical simulations and parametric study, our research investigates the eddy current forces, torques, and motion dynamics experienced by graphene flakes of different layers in an alternating magnetic field. The findings demonstrate that eddy current forces can overcome liquid-phase resistance, enabling controlled directional movement of graphene flakes. At a magnetic field frequency of 45 kHz, graphene flakes with fewer layers show enhanced settling velocities and quicker response times, suggesting a potential for statistically significant separation of graphene from impurities under the influence of the alternating magnetic field. This initial study

* Corresponding author at: School of Metallurgy, Northeastern University, Shenyang 110819, China.
** Corresponding authors.
E-mail addresses: ali@mail.neu.edu.cn, a.r.kamali@cantab.net (A.R. Kamali), wangq@mail.neu.edu.cn (W. Qiang), dmontalvao@bournemouth.ac.uk (D. Montalvão), aabdelkader@bournemouth.ac.uk (A. Abdelkader).
[1] These authors contributed equally as first author to this work.

https://doi.org/10.1016/j.powtec.2024.120561
Received 17 October 2024; Received in revised form 4 December 2024; Accepted 13 December 2024
Available online 15 December 2024

supports the feasibility of integrating eddy current separation technology into the graphene purification process, providing valuable insights for future research in this field.

1. Introduction

Graphene is a two-dimensional crystalline material composed of carbon atoms, exhibiting numerous unique physical and chemical properties. Its exceptional electrical conductivity arises from the honeycomb arrangement of carbon atoms, allowing electrons to move freely within the graphene lattice. As a result, graphene has found extensive applications in high-performance electronic devices [1]. Furthermore, graphene has the highest known tensile strength and elastic modulus, presenting diverse prospects in composite reinforcement, nanomechanics, and flexible electronics [2]. The exceptional biocompatibility of graphene also highlights its potential in the biomedical field, enabling applications like biosensors, drug delivery, and tissue engineering [3]. Additionally, graphene exhibits outstanding optical properties [4], thermal conductivity [5], and chemical stability [6], thus offering vast potential in optical devices, optoelectronics, thermal interface materials, thermoelectric devices, chemical sensors, corrosion-resistant coatings, touch screens, and more [7]. However, the exceptional properties of graphene are often dependent on thickness and considerably decline when the thickness of the flakes increases.

With the increasing number of applications and technological advancements, the demand for graphene is expected to increase rapidly, while large-scale production methods often struggle with product quality control [8,9]. Top-down approaches of graphene production implement layer separation by disrupting the interlayer structure within graphite to produce graphene flakes. Liquid-phase exfoliation (LPE) is among the most common and promising top-down approaches for the large-scale production of graphene [10]. This technique typically involves dispersing graphene in a solvent, followed by separating it from the solvent through methods such as centrifugation or filtration [11,12]. However, LPE still faces challenges in solvent selection and the subsequent purification of graphene [13], keeping aside the difficulties of separating the product based on the number of layers. In addition to the residual solvents, other common impurities associated with graphene might include carbon-based impurities like oxidised graphene and amorphous carbon, metal impurities such as Fe, Ni, Co, Cu, and non-metallic impurities such as silicates and oxides. These impurities as well as the presence of thick graphene, may potentially exert adverse effects on the electrical and electrochemical performance [9], affecting associated industrial applications of graphene [14].

Generally, the removal of impurities, and the separation of laeyered materials based on their thickness are conducted in two separate stages. Impurity removal usually occurs through acid washing [15] and organic solvent leaching processes [16], and might involve some additional vacuum and heat treatment steps [17,18]. Thickness-based separation of flakes is primarily based on isopycnic separation in a uniform or density gradient medium (DGM). The former is known as sedimentation-based separation (SBS) [19], while the latter is referred to as density gradient ultracentrifugation (DGU) [20]. SBS separates various particles based on the differences in sedimentation rates due to centrifugal forces. Sedimentation-based separation is the most common separation strategy successfully applied to flakes ranging from several nanometers to a few micrometres, with concentrations as high as a few mg/ml [21]. Larger flakes in a higher-viscosity medium experience greater friction, which reduces their sedimentation coefficient, making them less likely to settle. In the DGU process, flakes undergo ultracentrifugation until reaching their respective isopycnic point, where their buoyant density matches that of the surrounding medium. Additionally, surfactants can be added to enhance the density differences, where the buoyant density increases with the number of graphene layers [22]. Alternatively, DGU method may rely on the differences in sedimentation rates caused by particle size, shape, and mass variations to achieve separation, known as rate zonal separation (RZS). For example, larger particles settle at a faster rate [23].

These purification methods still face several challenges, such as the balance among efficiency, purity, and yield, as well as the impact of purification methods on the properties of graphene. The overlap between the flakes' thickness and the lateral dimensions raises doubts about the effectiveness of the isopycnic thickness separation. Non-contact physical separation methods, including those based on electrostatic forces, are commonly used in the mineral industry for purification and materials classification [24]. This non-contact approach typically involves no consumption of reagents and introduces no additional impurities. Graphene exhibits significantly higher electrical conductivity than various impurities, making it feasible to consider non-contact techniques to remove less conductive impurities. The significant variation in electrical conductivity among monolayer, bilayer and multilayer graphene allows techniques based on the difference in the electric conductivity, such as eddy current separation [25], to separate graphene flakes according to their number of layers. Since the eddy current separation is mainly based on the electric conductivity, the thickness separation should be independent of the flakes' lateral size. During the process of eddy current separation, conductive particles experience additional eddy current forces and torques, causing their trajectories to differ from those of non-conductive or low-conductivity particles, thus achieving separation. The crucial roles played by eddy current forces and torques in eddy current separators have found extensive applications in various fields, including mineral extraction [26], separation of fine particles [27], manipulation of space debris [28], eddy current couplers [29], and eddy current dampers [30]. However, to the best of our knowledge, no prior research has investigated the potential application of eddy current separation in the purification process of graphene.

Therefore, this study establishes a coupled simulation model of eddy current separation. Subsequently, we examine the influence of key factors such as the number of layers, radius and attitude angle of graphene flakes as well as the magnetic field frequency on eddy current forces and torques. Finally, we explore the motion of graphene flakes under the combined influences of gravity, eddy current forces, and liquid resistance, and analyze the shielding effect between two graphene flakes. The research can provide initial insights into the feasibility of purifying graphene using eddy current separation.

2. Models and methods

In order to explore the application of eddy current separation in the purification of graphene flakes, this study combines the finite element method (FEM) and computational fluid dynamics (CFD) to construct a coupled simulation model that can simulate the motion of particles. This section primarily introduces the coupled simulation model, its parameters validation, and the parametric study method.

2.1. Coupled simulation model for eddy current separation

Under an alternating magnetic field, graphene flakes in the liquid medium are subjected to eddy current forces, resistance, and gravity. The eddy current forces acting on the graphene flakes were obtained through ANSYS Maxwell, and subsequently, the data of the forces were imported into ANSYS Fluent. This enables the simulation of the movement of graphene flakes under various forces.

In ANSYS Maxwell, graphene flakes are placed in an alternating magnetic field, and a three-dimensional transient solver [25,31] was

used to calculate the eddy current forces acting on the graphene flakes, as shown in Fig. 1 (a). The vector gradient of the magnetic field [32] in the simulation model is approximately 6.6×10^4 T/m, the magnetic flux density is about 0.512 T, and the magnetic field frequency can be adjusted as needed. The graphene flakes were assumed to have a circular sheet-like shape, with specific geometric and physical parameters set based on literature [33] and the applicability of the model (see Table 1). Notably, the electrical conductivity of graphene decreases with an increase in the number of graphene layers. Moreover, the radius and the attitude angle (α) about the x-axis are also the factors considered in this study.

The simulation of graphene flake movement in a solution after loading eddy current force was conducted using Fluent. User-defined functions (UDF) were employed to load data related to the mass and eddy current forces, and a six degrees of freedom (6DOF) solver was utilised to simulate graphene flake movement. The 6DOF solver, based on the dynamic mesh, can calculate the movement of objects in a liquid/gas medium under the influence of drag, gravitational, and other forces. These forces are determined through numerical integration of pressure and shear stress on the structure surface. Moreover, the 6DOF solver can apply additional forces to particles, such as jet forces, thrust, and electromagnetic forces. The control equations for solving the translational motion of the center of mass in an inertial coordinate system are as follows:

$$\dot{\vec{v}}_G = \frac{1}{m}\sum \vec{f}_G \tag{1}$$

where $\dot{\vec{v}}_G$ is the translational acceleration of the center of mass, $\vec{v}_G$ represents the translational velocity vector of the moving object, m is the mass of the rigid body, and $\vec{f}_G$ is the force vector. Utilizing the local coordinate system of the object itself is more suitable for the rotational motion of the object:

$$\dot{\vec{\omega}}_B = L^{-1}\left(\sum \vec{M}_B - \vec{\omega}_B \times L\vec{\omega}_B\right) \tag{2}$$

where $\dot{\vec{\omega}}_B$ represents the angular acceleration of the center of mass, L is the inertia tensor of the rigid body, $\vec{M}_B$ is the torque vector, and $\vec{\omega}_B$ represents the angular velocity vector of the moving object. Building upon this foundation, the translational velocity and angular velocity of the moving object can be determined using a fourth-order Adams-Moulton equation:

$$x^{k+1} = x^k + \frac{\Delta t}{24}(9\dot{x}^{k+1} + 19\dot{x}^k - 5\dot{x}^{k-1} + \dot{x}^{k-2}) \tag{3}$$

where x represents either $\vec{\omega}_B$ or $\dot{\vec{v}}_G$, and the computed results will subsequently be incorporated into the process of dynamic meshing [34]. Through this coupled model, our study can conveniently acquire information about the eddy current forces, torques, and motion states experienced by graphene flakes in an alternating magnetic field for various conditions.

Table 1
Parameters used in the coupling simulation model.

Factors	Values					
Attitude angle (°)	0–180					
Radius (μm)	0.75–12					
Magnetic field frequency	45 kHz-450 GHz					
Number of layers	1	2	4	8	10	150
Thickness (nm)	0.34	0.68	1.36	2.72	3.4	51
Conductivity (MS/m)	100	79	39	20	10	1

2.2. Verification of model parameters

To ensure that the computational load and accuracy of the numerical simulations are within reasonable limits, parameters such as time step and mesh used in the simulation model were determined through independent verification. The coupled simulation model used in this study primarily explores the application of eddy current separation in the purification process of graphene. The simulation cases involve geometric structures with sub-nanometer thickness, posing significant challenges for the model setup due to the extremely high aspect ratio of the structures. Thus, an adaptive mesh was used in the coupled simulation model. In this configuration, the adaptive mesh generated by the magnetostatic solver was imported into the transient solver. Conventional geometric structures typically do not require significant adjustments to preset meshing parameters. However, different preset meshing parameters were tested for these ultra-thin structures to compare the changes in eddy current forces over time, as shown in Fig. 2 (a).

The results demonstrated that when the number of elements reached 900,000, the accuracy was comparable to cases with higher element numbers. Therefore, the preset meshing parameters corresponding to the magnitude of 900,000 were employed in the model. In the case with 418 k elements, an insufficient number of mesh elements can result in mesh elements that also have a high aspect ratio. It can lead to inadequate resolution or convergence issues, as it fails to accurately capture the variations in the electromagnetic fields. Similarly, the independence verification for the time step in the model was also conducted, determining a time step of 3 ns, as shown in Fig. 2 (b).

2.3. Parametric study method

This study considers four factors: the number of layers, magnetic field frequency, radius, and attitude angle. Since the number of layers is a discrete variable, the parametric study focused on the remaining three factors: magnetic field frequency, radius, and attitude angle. A central composite design (CCD) with three variables at five levels was implemented using the Design Expert software. The actual and coded values for the independent variables are listed in Table 2.

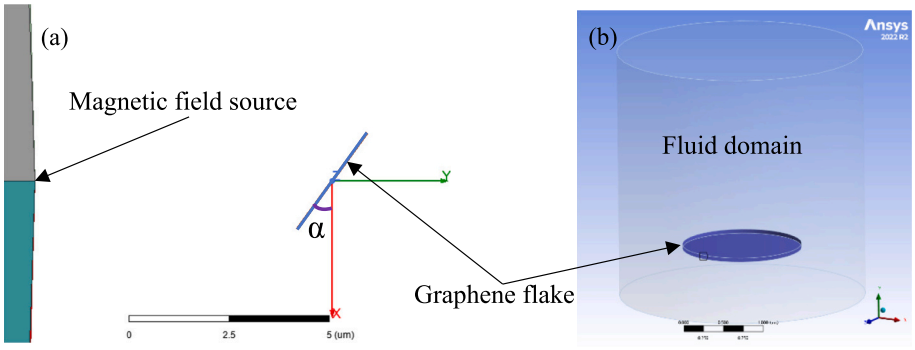

Fig. 1. Coupling simulation model of eddy current separation: (a) Three-dimensional transient simulation model in Maxwell; (b) Simulation model in Fluent.

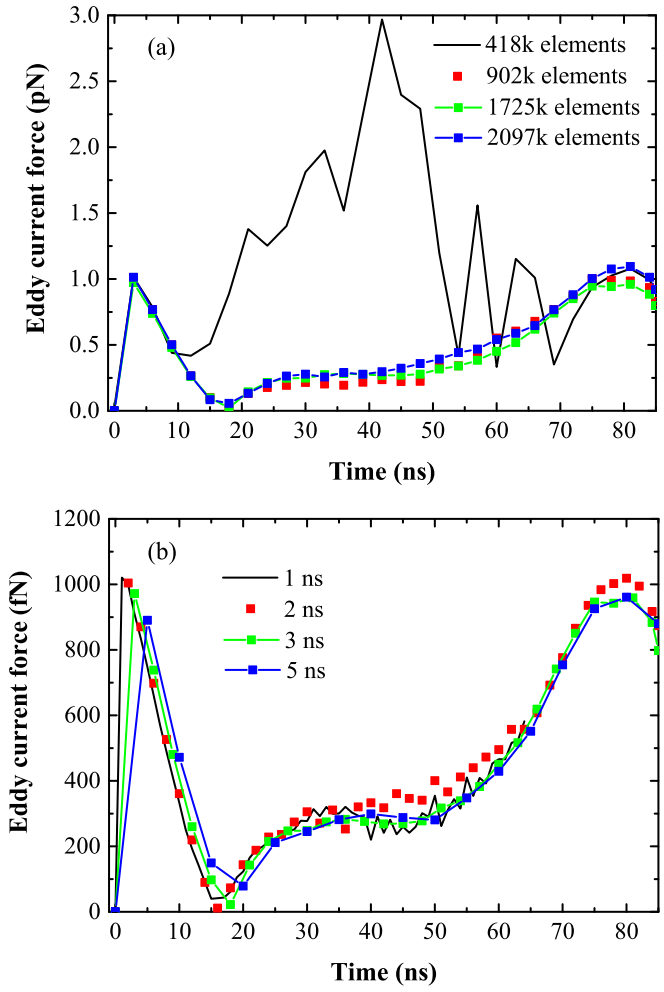

Fig. 2. Variation of eddy current force with time under different element numbers and time step parameters.

It is important to note that simulations involving few-layer graphene with a radius of 12 μm required significant computational resources. The extremely high aspect ratio of graphene with a large radius and small thickness results in a high mesh density requirement for sufficient accuracy, exceeding the capacity of our computational equipment. To address this, the number of layers in the parametric study was fixed at 150, substantially reducing the computational load and enabling the simulations to proceed. The experimental design consisted of 13 runs covering a wide range of parameters, including three repeated experiments at the center of the factor space, as summarized in Table 3.

A second-order polynomial equation was fitted to the simulation results, and the empirical model derived through multiple regression analysis were employed to predict the response, namely the average eddy current force ($\overline{F_{eddy}}$), across the entire factor space. To validate the regression model correlating the response to the variables, statistical tests were performed, including analysis of variance (ANOVA) and an R^2 analysis, which measures the proportion of explained variation relative to the total variation. Finally, the optimal parameters can be obtained directly by using response surface analysis.

3. Results and discussion

3.1. Electromagnetic forces on graphene flakes

During the process of eddy current separation, conductive particles in an alternating magnetic field experience the influence of eddy current forces and torques, enabling the separation of materials with different electrical conductivities [35]. Eddy current forces and torques can cause translational and rotational motion in conductive particles. Therefore, these forces and torques play a crucial role in determining the feasibility of separation and purification in eddy current separation processes. In this section, we examine the impact of factors such as the number of graphene layers and the magnetic field frequency on the eddy current forces and torques.

Fig. 3(a) illustrates the variation of the average eddy current force with respect to the number of graphene layers at different magnetic field frequencies. It can be seen that the number of graphene layers does not significantly influence the absolute value of the eddy current forces acting on graphene flakes. According to our previous research [32], the eddy current force and torque are the resultant of Lorentz forces generated by the interaction between a magnetic field and the eddy currents. Thus, the eddy current force and torque are proportional to the eddy currents. In addition, the equivalent resistance of a graphene flake is inversely proportional to its conductivity and thickness. When the number of graphene layers increases from 1 to 150, the decrease in conductivity increases the equivalent resistance, while the increase in thickness reduces it. Consequently, as the number of graphene layers increases, the electrical conductivity gradually decreases, reducing eddy current forces. Simultaneously, the increase in thickness can enhance the magnitude of the eddy current forces. These two mechanisms offset each other, resulting in the absence of a significant trend in the eddy current forces as the number of layers varies. Nevertheless, due to the proportional relationship between the mass of graphene flakes and their number of layers, the acceleration of average eddy current forces gradually decreases with an increase in the number of graphene layers, as illustrated in Fig. 3(b). This indicates that single-layer graphene

Table 3
Design and results of the simulation.

Run	Factors			Responses
	X_1(°)	X_2(kHz)	X_3(μm)	$\overline{F_{eddy}}$ (pN)
1	153.64	3.84099E+9	2.39752	417,962
2	153.64	6.5901E+8	10.3525	2.49702E+7
3	26.3604	3.84099E+9	10.3525	4.06619E+7
4	26.3604	6.5901E+8	2.39752	105,824
5	0	2.25E+9	6.375	8.24582E+6
6	180	2.25E+9	6.375	8.28216E+6
7	90	45	6.375	0.351839
8	90	4.5E+9	6.375	1.76236E+7
9	90	2.25E+9	0.75	3114.78
10	90	2.25E+9	12	1.39197E+8
11	90	2.25E+9	6.375	1.26658E+7
12	90	2.25E+9	6.375	1.25883E+7
13	90	2.25E+9	6.375	1.26465E+7

Table 2
Actual and coded values in central composite design.

Variable (unit)	Symbol	Coded values				
		−1.41421	−1	0	1	1.41421
Attitude angle (°)	X_1	0	26.3604	90	153.64	180
Frequency (kHz)	X_2	45	6.5901E+8	2.25E+9	3.84099E+9	4.5E+9
Radius (μm)	X_3	0.75	2.39752	6.375	10.3525	12

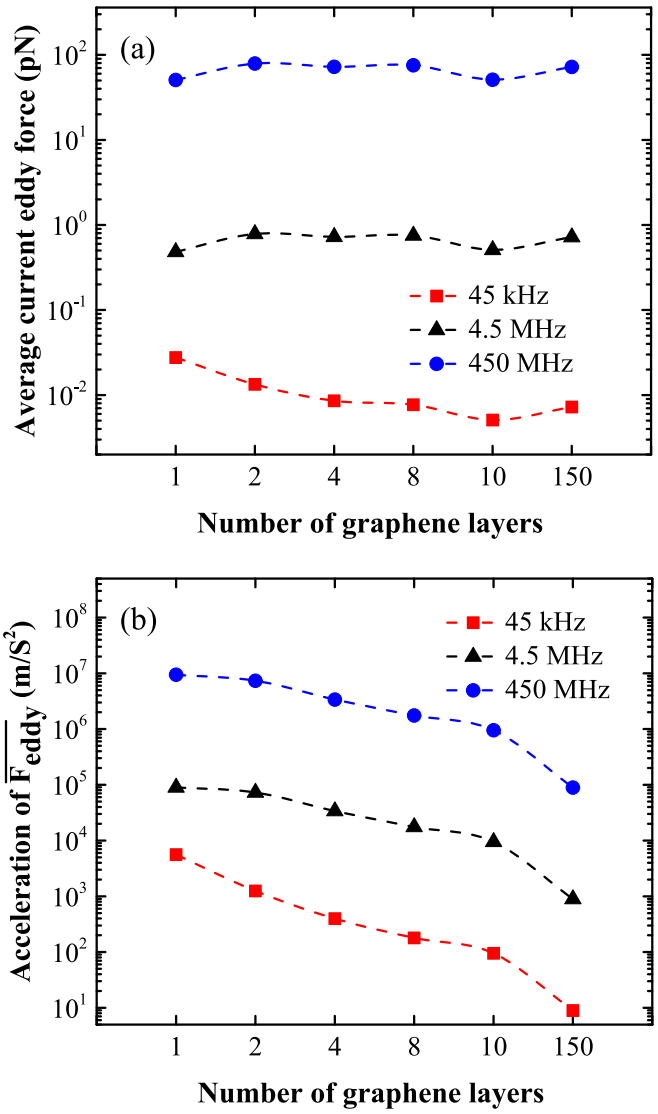

Fig. 3. Variation of the average eddy current force (a) and its acceleration (b) in response to the number of graphene layers under different magnetic field frequencies.

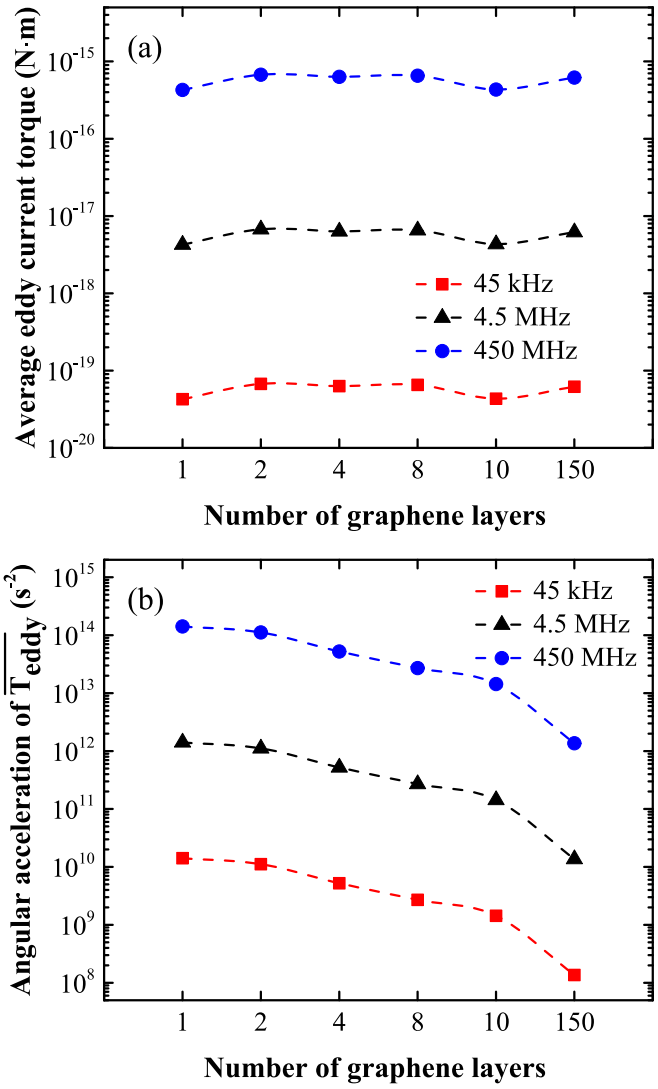

Fig. 4. Variation of the average eddy current torque (a) and its angular acceleration (b) with respect to the number of graphene layers under different magnetic field frequencies.

exhibits a superior response rate to eddy current forces compared to the graphene flakes with more layers.

Fig. 4 depicts the changes in the average eddy current torque ($\overline{T_{eddy}}$) and its angular acceleration with respect to the number of graphene layers under different magnetic field frequencies. It can be demonstrated that the eddy current torque and its angular acceleration exhibit patterns similar to those observed for the eddy current force and the acceleration, indicating that the mechanisms explaining the variation in the eddy current force are equally applicable to the eddy current torque. Additionally, Fig. 3 and Fig. 4 illustrate that the eddy current force and acceleration, along with the eddy current torque and its angular acceleration, increase as the magnetic field frequency rises. The change rate of the magnetic field over time can influence the magnitude of eddy currents, thus affecting both eddy current force and torque. This is consistent with the findings of our previous research [32]. In practical applications, adjusting the magnetic field frequency offers a means to modulate the magnitude of eddy current forces and torque, thereby enabling control over the rates of separation or purification.

The eddy current forces experienced by graphene flakes during the rotational motion induced by the eddy current torque were also investigated. Fig. 5(a) shows the variation of the average eddy current force on single-layer graphene as a function of attitude angle at a magnetic field frequency of 4.5 MHz. It reveals that the average eddy current force exhibit fluctuations with changes in the attitude angle of the graphene flake, albeit with a relatively small amplitude. This suggests the attitude angle of graphene flake does not significantly impact the final separation or purification during the purification process of graphene. Fig. 5(b) shows the variation in the average eddy current force with the radius of graphene flake at a magnetic field frequency of 4.5 MHz. The results demonstrate that the average eddy current forces linearly increase with increasing the flake's lateral size. Fig. 5(c) illustrates the variation of the average eddy current force across magnetic field frequencies ranging from 45 to 4.5 × 10^9 kHz. Similar to the influence of radius on the eddy current force, increasing the magnetic field frequency significantly enhances the eddy current force acting on the graphene flake, consistent with the results shown in Fig. 3. A closer examination of the data reveals subtle trends not immediately evident in the figure. Within the frequency range of 45 to 4.5 × 10^7 kHz, the eddy current force increases by approximately 98-fold for every two orders of magnitude increase in frequency. However, when the frequency rises from 4.5 × 10^7 to 4.5 × 10^9 kHz, the eddy current force increases by only about 65-fold. This indicates a deceleration in the growth rate of the eddy current force. This phenomenon may be attributed to the decreasing skin depth, which

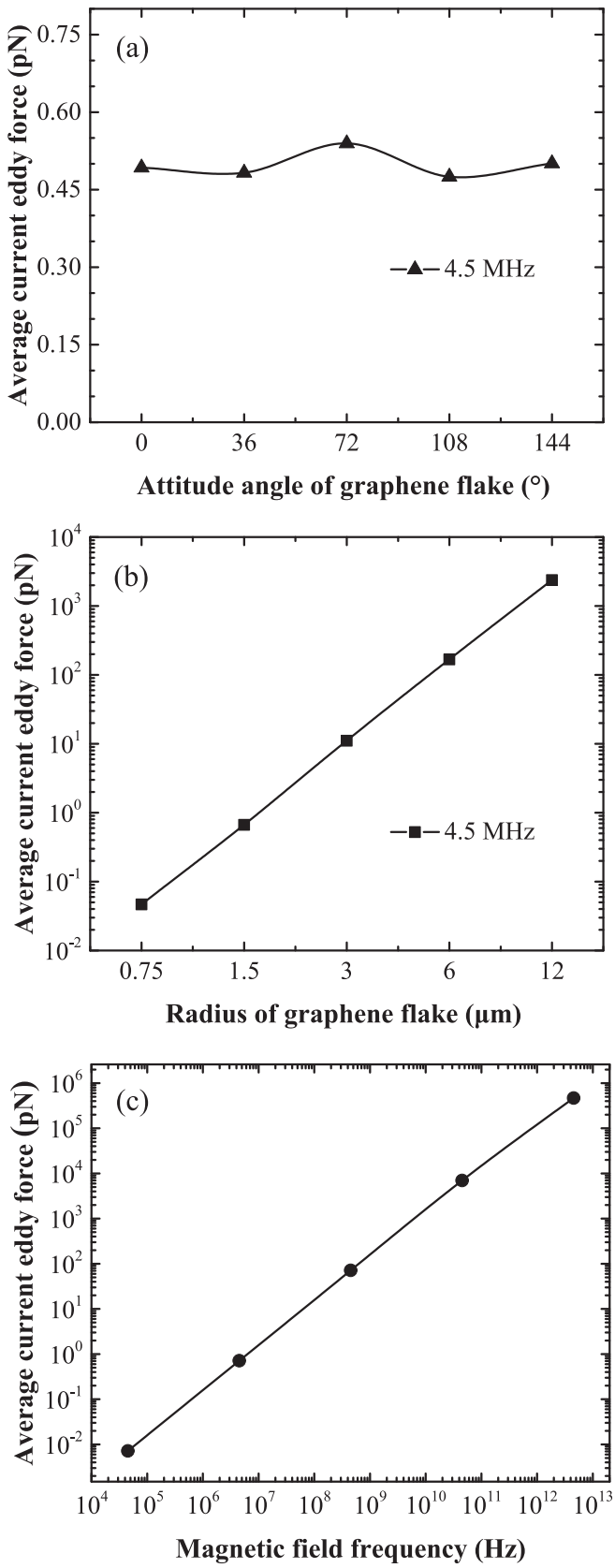

Fig. 5. (a) Variation of the $\overline{F_{eddy}}$ with the attitude angle for a single-layer graphene flake at 4.5 MHz; (b) Variation of the $\overline{F_{eddy}}$ with the radius of a 150-layer graphene flake at 4.5 MHz; (c) Variation of the $\overline{F_{eddy}}$ with the magnetic field frequency for a 150-layer graphene flake with a radius of 1.5 μm.

gradually approaches the thickness of the graphene flake as the magnetic field frequency increases, thereby slowing the growth rate of the eddy current force.

According to Stokes' law ($F_{\mathrm{drag}} = 6\pi\eta\upsilon R$), the resistance experienced by particles in a liquid medium is closely related to their particle size. Consequently, larger graphene flakes experience greater eddy current forces and resistances. Therefore, employing distinct magnetic field parameters for graphene flakes within different size ranges is advisable. The selection of these parameters can be guided by previous research concerning the influence of particle size on eddy current separation [25], recommending the use of larger magnetic field gradients and frequencies for smaller particles.

3.2. Parametric study of eddy current force

The eddy current force is a critical technical parameter for this purification technique; therefore, we conducted a parameter study on it. Based on the various parameter combinations of the three factors and the corresponding simulation results presented in Table 3, a reduced second-order regression model for $\overline{F_{eddy}}$ was derived using the stepwise regression method. The resulting model, expressed in terms of the actual factors, are formulated as follows.

$$\overline{F_{eddy}}^{0.5} = -1787.6673 + 1.5041 \bullet 10^{-6} \bullet X_2 + 27.0525 \bullet X_3 + 1.0310 \bullet 10^{-8} \bullet X_1 \bullet X_2 + 1.9119 \bullet X_1 \bullet X_3 - 0.2002 \bullet {X_1}^2 - 3.7330 \bullet 10^{-16} \bullet X_2^2 + 61.2457 \bullet X_3^2 \quad (4)$$

The analysis of variance (ANOVA), summarized in Table 4, reveals that the regression model is highly significant, with an F-value of 113.85 and a *p*-value less than 0.0001. The model's fitting performance was assessed using R^2 and $Adj.R^2$. The high values of R^2 (0.9938) and $Adj.R^2$ (0.9850) demonstrate an excellent fit between the regression model and the simulation data, indicating that the model effectively accounts for the majority of the variability in the results. Furthermore, the close agreement between R^2 and $Adj.R^2$ suggests that the likelihood of the model containing insignificant terms is negligible.

The plot of predicted versus actual values (Fig. 6) demonstrates a strong consistency between the two, indicating that the regression models possess robust predictive capabilities. The coefficient of variation (C.V.), a dimensionless metric representing the standard deviation as a percentage of the mean, provides a measure of experimental accuracy. The C.V. value for the regression model is 11.36 % (Table 4),

Table 4
Analysis of variance and statistical parameters for the regression model.

Source	Sum of squares	Degrees of freedom	Mean square	F-value	p-value
Model	1.222E+8	7	1.745E+7	113.85	< 0.0001
X_2	8.809E+6	1	8.809E+6	57.46	0.0006
X_3	6.894E+7	1	6.894E+7	449.69	< 0.0001
X_1X_2	4.812E+6	1	4.812E+6	31.39	0.0025
X_1X_3	2.242E+6	1	2.242E+6	14.63	0.0123
X_1^2	1.786E+6	1	1.786E+6	11.65	0.0190
X_2^2	5.510E+6	1	5.510E+6	35.94	0.0019
X_3^2	6.987E+6	1	6.987E+6	45.58	0.0011
Residual	7.666E+5	5	1.533E+5		
Lack of fit	7.665E+5	3	2.555E+5	7934.83	0.0001
Pure Error	64.40	2	32.20		
Cor Total	1.229E+8	12			

$R^2 = 0.9938$ $Adj.R^2 = 0.9850$ $C.V. = 11.36$ % Adeq Precision = 38.4091.
R^2: Coefficient of determination, *C.V.*: Coefficient of variation.

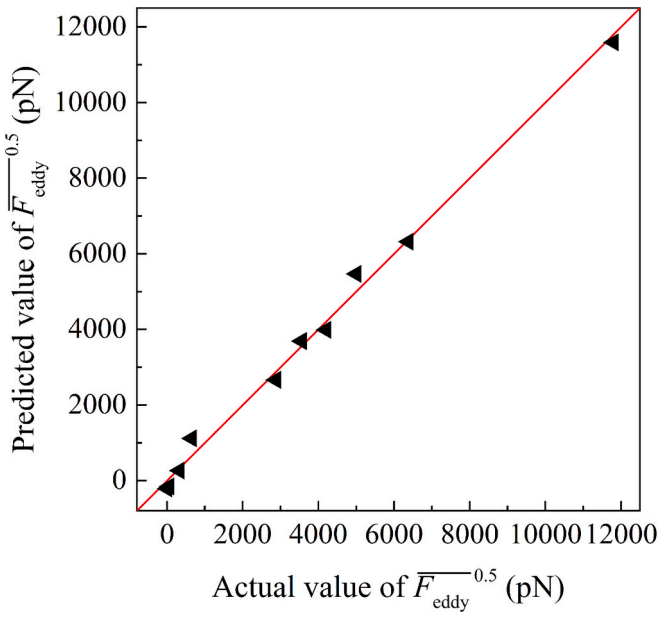

Fig. 6. Predicted vs. actual values plot for $\overline{F_{eddy}}^{0.5}$.

suggesting that the simulation results are reliable and exhibit good reproducibility. However, this also highlights a limitation in the adequacy of the regression model. Specifically, the lack-of-fit *p*-value in the ANOVA analysis is only 0.0001, which may point to insufficient model adequacy. Similar statistical patterns have been observed in the simulation studies by Wang et al. [36] and Cao et al. [35].

Based on the regression model, the optimal parameter combination was obtained through response surface analysis: when the attitude angle is 180°, the magnetic field frequency is 4.5×10^9 kHz, and the radius is 12 μm, the eddy current force reaches 2.58704×10^8 pN. This result is consistent with the findings of the single-factor analysis in Fig. 5, indicating that increasing the magnetic field frequency and radius can enhance the eddy current force.

To further analyze the applicability of the above parameter study to graphene flakes with different layer numbers, it is necessary to discuss the interaction effects between the number of layers and the three factors: radius, magnetic field frequency, and the attitude angle. Among these factors, the magnetic field frequency is the most likely to interact with the number of graphene layers due to the skin effect. However, the results in Figs. 3 and 4 show no significant interaction between magnetic field frequency and the number of layers. To investigate this further, the skin depth was calculated. Using the formula for the skin effect, the calculated skin depths under the maximum frequency of 4.5×10^9 kHz for graphene layers with 1, 2, 4, 8, 10, and 150 layers are 0.0237, 0.0267, 0.0380, 0.0531, 0.0750, and 0.2373 μm, respectively. These values are all much larger than the thickness of the corresponding graphene flakes. Therefore, the influence of the skin effect is negligible under the current operating conditions, which explains the lack of significant interaction between magnetic field frequency and the number of layers. Based on this analysis, the optimized parameters derived for 150-layer graphene provide valuable guidance for graphene flakes with other layer numbers as well.

3.3. Feasibility analysis of the purification technology

To further validate whether an alternating magnetic field significantly affects the motion state of graphene flakes, it is essential to investigate whether the eddy current force acting on the graphene flake can have a noticeable impact on the motion trajectory. Therefore, the application of eddy current forces to the motion profile of graphene flakes in Fluent was implemented using UDF.

Fig. 7 illustrates the changes in the position and motion state of a 10-layer graphene flake after applying eddy current forces. The figure shows that the eddy current force can overcome the liquid-phase resistance experienced by the graphene flake and drive its motion. Similar phenomena were observed in simulated cases involving graphene flakes with different numbers of layers. These results provide theoretical evidence supporting the feasibility of applying eddy current separation technology to the purification of graphene.

As eddy current forces are applied to graphene flakes, the flakes initiate an accelerating motion, increasing the velocity. According to Stokes' law, the liquid-phase resistance experienced by the particles increases with their velocity. This suggests the graphene flakes subjected to the eddy current forces are accelerated, and the acceleration continues until a point of equilibrium is reached, where the resultant force is zero. At this equilibrium, the particle's velocity can be referred to as the settling terminal velocity. The magnitude of the settling terminal velocity primarily depends on the magnitude of the eddy current force.

Table 5 presents the average eddy current force and the response time of graphene flakes to travel a distance of 5 μm for different numbers of layers at a magnetic field frequency of 45 kHz. It shows a significant variation in the average eddy current forces for graphene flakes with different numbers of layers. Consequently, these graphene flakes exhibit notable differences in settling terminal velocities and response times. Specifically, graphene flakes with fewer layers exhibit higher settling terminal velocities and faster response rates. This indicates that when subjected to an alternating magnetic field, graphene flakes with a specific number of layers have the potential to form higher concentration enrichments in specific regions, achieving statistically significant separation of graphene flakes with different numbers of layers.

In the large-scale preparation of graphene, the solution contains a large number of graphene flakes. When subjected to an alternating magnetic field, the graphene flakes may interact with each other, potentially jeopardizing the feasibility of the purification technology. Therefore, we investigated a case involving two graphene flakes and compared the eddy current forces between this case and a single graphene flake case. This comparison allowed us to clarify whether the presence of other graphene flakes shielding the magnetic field would significantly affect the eddy current force on the shielded graphene flake.

Compared to the single graphene flake case, the two-graphene-flake case involves a single-layer graphene flake and a magnetic field source with identical parameters, while the shielding graphene flake is positioned between the magnetic field source and the single-layer graphene flake, as shown in Fig. 8(a). To thoroughly investigate the shielding effect of the graphene flake, we conducted simulation cases with shielding graphene flakes under different radii and layer numbers and obtained the eddy current force on the shielded graphene flake.

Fig. 8(b) shows the variation of the eddy current force with the radius of the shielding graphene flake (with 4 layers) under a magnetic field frequency of 4.5 MHz. Fig. 8(c) illustrates the variation of the eddy current force with the number of layers of the shielding graphene flake (with a radius of 1.5 μm) under the same magnetic field frequency. The red line in the figures represents the case with only one graphene flake, used for comparison. The results show that when graphene flakes of different thicknesses and radii are placed between the magnetic field source and other graphene flakes, they do not significantly affect the eddy current force on the other graphene flakes. In other words, the shielding graphene flakes cannot isolate the effect of the magnetic field source on the graphene flakes located behind them. As mentioned in Section 3.2, within the parameter range of this study, the thickness of the graphene flakes is smaller than their skin depth, resulting in a very limited magnetic shielding effect.

These findings demonstrate the possibility of extending the eddy current separation technology to purify graphene products. However, the hardware facilities for experimental validation are currently

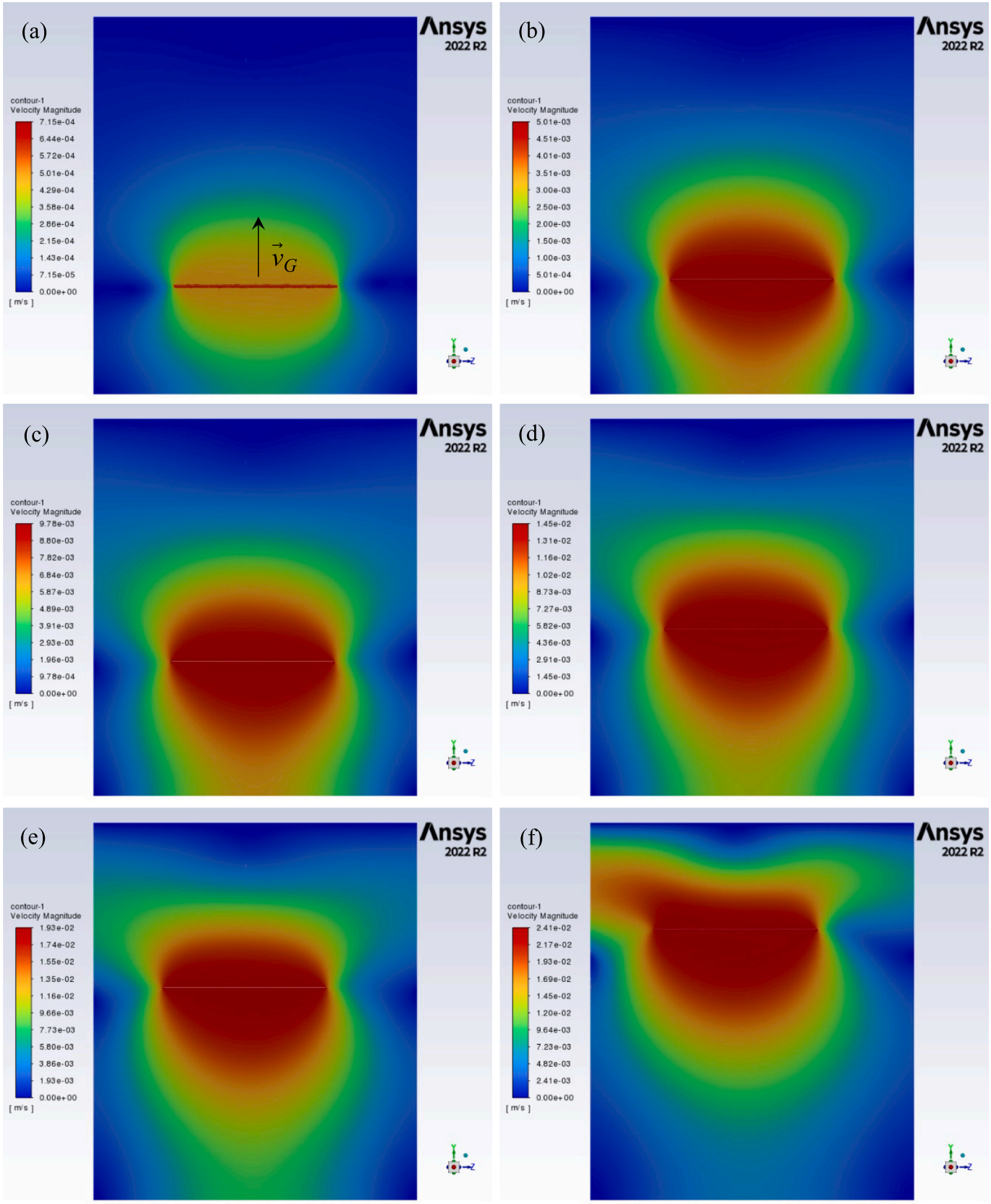

Fig. 7. The motion state of a 10-layer graphene flake at different moments: (a) 5.0×10^{-6} s; (b) 5.0×10^{-5} s; (c) 1.0×10^{-4} s; (d) 1.5×10^{-4} s; (e) 2.0×10^{-4} s; (f) 2.5×10^{-4} s.

Table 5
Eddy current force and response time of graphene flakes in an alternating magnetic field.

Number of graphene layers	1	2	4	8	10	150
$\overline{F_{eddy}}$ (N × 10^{-15})	30.15	13.38	8.56	7.72	5.10	7.24
Time (s × 10^{-5})	4.05	8.90	15.60	23.40	32.00	104.80

insufficient. It is important to note that the vector gradient of the magnetic field, the magnetic flux density, and frequency were considered to be approximately 6.6 × 10^4 T/m, 0.512 T and 45 kHz, respectively. The magnetic flux density or magnetic field frequency parameters are relatively straightforward to achieve, but the high vector gradient of the magnetic field pose certain technical challenges. Compared to the traditional eddy current separation, the purification method of graphene explored in this study is also grounded in exploiting the variations in the electrical conductivity of materials, utilizing the eddy current forces induced by an alternating magnetic field to separate different materials. Hence, both techniques fall under the category of eddy current separation technology. However, several distinctions set the purification method apart. Firstly, traditional eddy current separators typically handle "three-dimensional" particles with substantial thickness, while graphene flakes are extremely thin and belong to the "two-dimensional" region. Additionally, traditional eddy current separators are designed for processing materials in the millimeter range, whereas the graphene purification method reported here primarily targets materials at the micrometer scale. Moreover, conventional eddy current separators usually operate in gaseous mediums for separation, while the graphene purification method discussed uses liquid-phase mediums. Furthermore, the magnetic field gradients and frequencies employed in the traditional eddy current separation are relatively low, whereas the graphene purification method requires much higher magnetic field gradients and frequencies. Lastly, traditional eddy current separators are commonly utilised in the recovery stage of non-ferrous metals from solid wastes, while the purification method is applied in the preparation stage of graphene. These distinctions highlight the unique characteristics and requirements of the purification process of graphene, making it a tailored application of eddy current separation technology. It is worth noting that the eddy current forces and torques discussed in this study not only hold potential applications in the purification process of graphene but also exhibit applicability in the realm of graphene transport or transfer [22]. The results obtained will be employed to design an eddy current purification set-up exploring the findings of this article experimentally, and results will be reported in subsequent reports.

4. Conclusions

In this study, we investigated the forces applied to, and the subsequent motion of, graphene flakes with varying number of layers in an alternating magnetic field through numerical simulations and a parametric study. The results show that the eddy current forces on the graphene flakes increase with the magnetic field frequency and radius. The eddy current forces are sufficient to overcome the liquid-phase resistance or gravity, thereby driving the graphene flakes to undergo directional motion. The results also indicate that the shielding effect between graphene flakes is limited. The preliminary findings suggest the potential application of eddy current separation for the purification of graphene. Furthermore, graphene flakes with different number of layers experience varying magnitudes of eddy current forces at suitable magnetic field frequencies. This suggests that the separation of graphene flakes in an alternating magnetic field based on their number of layers may be feasible. In short, this study provides valuable possibilities for further exploration of eddy current force-based purification of 2D materials, and offers technical guidance for subsequent experimental investigations.

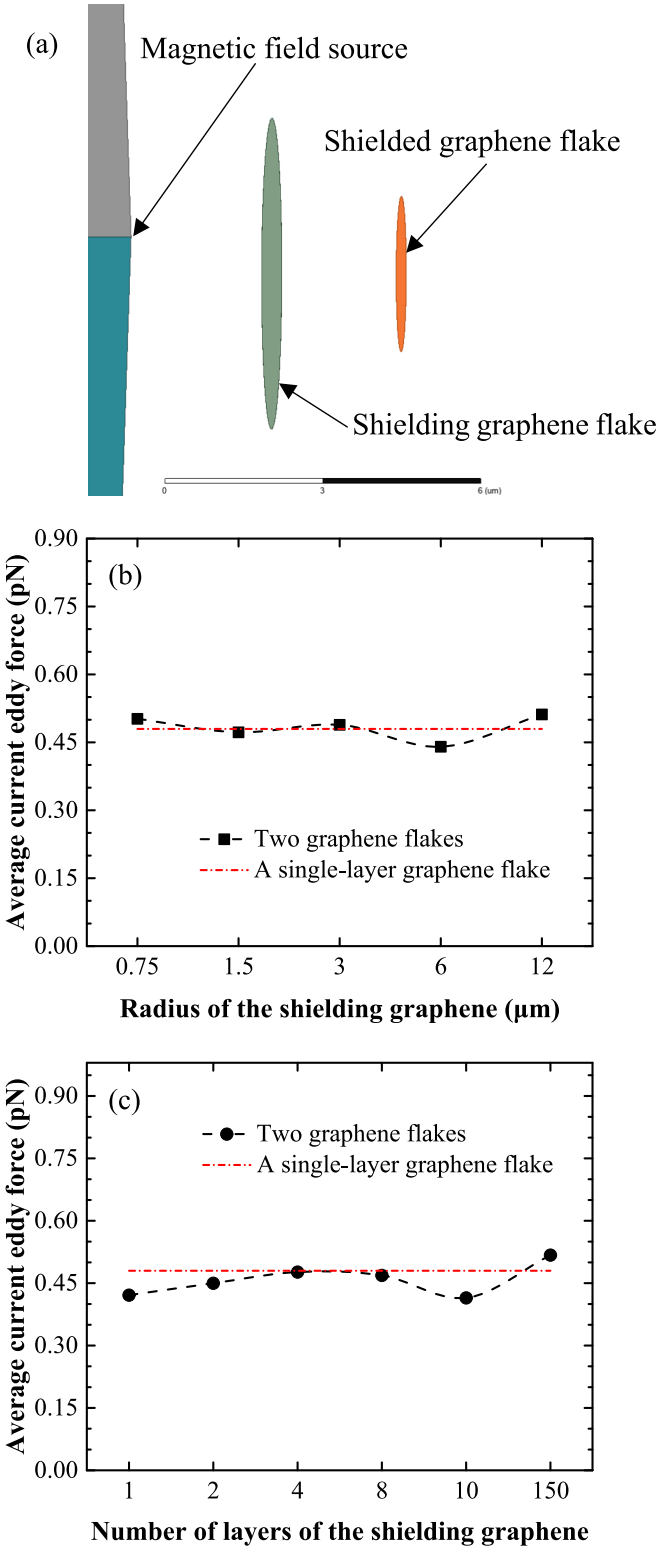

Fig. 8. (a) The simulation model containing two graphene flakes; (b) The average eddy current force of the shielded graphene flake as a function of the radius of the shielding graphene; (c) The average eddy current force of the shielded graphene flake as a function of the number of layers of the shielding graphene.

CRediT authorship contribution statement

Cao Bin: Writing – review & editing, Writing – original draft, Visualization, Validation, Software, Methodology, Investigation, Data curation, Conceptualization. **Yuan Yi:** Writing – review & editing, Visualization, Supervision, Resources, Project administration, Funding acquisition, Formal analysis, Data curation, Conceptualization. **Shan Zhicheng:** Visualization, Software, Formal analysis, Data curation. **Yang Lixue:** Visualization, Validation, Software, Formal analysis. **Ali Reza Kamali:** Writing – review & editing, Visualization, Supervision, Resources, Project administration, Methodology, Funding acquisition, Formal analysis, Conceptualization. **Wang Qiang:** Visualization, Supervision, Software, Resources, Project administration, Funding acquisition, Formal analysis, Conceptualization. **Diogo Montalvão:** Supervision, Software, Resources, Project administration, Funding acquisition, Formal analysis. **Amor Abdelkader:** Writing – review & editing, Visualization, Supervision, Resources, Project administration, Methodology, Investigation, Funding acquisition, Formal analysis.

Declaration of competing interest

The authors declare that they have no known competing financial interests or personal relationships that could have appeared to influence the work reported in this paper.

Acknowledgments

The authors are grateful to the financial support provided by the National Natural Science Foundation of China (Grant Nos. 52274407, U21A20399, U21A20117, 52250610222). Cao Bin holds a scholarship provided by the China Scholarship Council during the study at Bournemouth University. The authors want to acknowledge Research England (United Kingdom) through the ADDSONIC's Bournemouth University Strategic Inevistment Area.

Data availability

Data will be made available on request.

References

[1] R. You, Y.Q. Liu, Y.L. Hao, D.D. Han, Y.L. Zhang, Z. You, Laser fabrication of graphene-based flexible electronics, Adv. Mater. 32 (2020) 1901981.
[2] D.G. Papageorgiou, I.A. Kinloch, R.J. Young, Mechanical properties of graphene and graphene-based nanocomposites, Prog. Mater. Sci. 90 (2017) 75–127.
[3] R. Boroujerdi, A. Abdelkader, R. Paul, Highly sensitive and selective detection of the antidepressant amitriptyline using a functionalised graphene-based sensor, ChemNanoMat 8 (2022) e202200209.
[4] V. Kumar, Linear and nonlinear optical properties of graphene: a review, J. Electron. Mater. 50 (2021) 3773–3799.
[5] H. Lin, Q. Jian, X. Bai, D. Li, Z. Huang, W. Huang, S. Feng, Z. Cheng, Recent advances in thermal conductivity and thermal applications of graphene and its derivatives nanofluids, Appl. Therm. Eng. 218 (2023) 119176.
[6] H.Y. Mao, Y.H. Lu, J.D. Lin, S. Zhong, A.T.S. Wee, W. Chen, Manipulating the electronic and chemical properties of graphene via molecular functionalization, Prog. Surf. Sci. 88 (2013) 132–159.
[7] F. Zhang, K. Yang, G. Liu, Y. Chen, M. Wang, S. Li, R. Li, Recent advances on graphene: synthesis, properties and applications, Compos. A: Appl. Sci. Manuf. 160 (2022) 107051.
[8] J. Zhang, K. Jia, L. Lin, W. Zhao, H.T. Quang, L. Sun, T. Li, Z. Li, X. Liu, L. Zheng, Large-area synthesis of superclean graphene via selective etching of amorphous carbon with carbon dioxide, Angew. Chem. Int. Ed. 58 (2019) 14446–14451.
[9] A. Ambrosi, M. Pumera, The CVD graphene transfer procedure introduces metallic impurities which alter the graphene electrochemical properties, Nanoscale 6 (2014) 472–476.
[10] X.J. Lee, B.Y.Z. Hiew, K.C. Lai, L.Y. Lee, S. Gan, S. Thangalazhy-Gopakumar, S. Rigby, Review on graphene and its derivatives: synthesis methods and potential industrial implementation, J. Taiwan Inst. Chem. Eng. 98 (2019) 163–180.
[11] F. Torrisi, T. Hasan, W. Wu, Z. Sun, A. Lombardo, T.S. Kulmala, G.W. Hsieh, S. Jung, F. Bonaccorso, P.J. Paul, D. Chu, A.C. Ferrari, Inkjet-printed graphene electronics, ACS Nano 6 (2012) 2992–3006.
[12] Y. Hernandez, V. Nicolosi, M. Lotya, F.M. Blighe, Z. Sun, S. De, I.T. McGovern, B. Holland, M. Byrne, Y.K. Gun'Ko, J.J. Boland, P. Niraj, G. Duesberg, S. Krishnamurthy, R. Goodhue, J. Hutchison, V. Scardaci, A.C. Ferrari, J. N. Coleman, High-yield production of graphene by liquid-phase exfoliation of graphite, Nat. Nanotechnol. 3 (2008) 563–568.
[13] L. Li, M. Zhou, L. Jin, L. Liu, Y. Mo, X. Li, Z. Mo, Z. Liu, S. You, H. Zhu, Research progress of the liquid-phase exfoliation and stable dispersion mechanism and method of graphene, Front. Mater. 6 (2019) 325.
[14] A. Ambrosi, S.Y. Chee, B. Khezri, R.D. Webster, Z. Sofer, M. Pumera, Metallic impurities in graphenes prepared from graphite can dramatically influence their properties, Angew. Chem. Int. Ed. 51 (2012) 500–503.
[15] S. Vivekchand, A. Govindaraj, A new method of preparing single-walled carbon nanotubes, J. Chem. Sci. 115 (2003) 509–518.
[16] D.P. Hansora, N.G. Shimpi, S. Mishra, Graphite to graphene via graphene oxide: An overview on synthesis, properties, and applications, JOM 67 (2015) 2855–2868.
[17] E. Stolyarova, K.T. Rim, S. Ryu, J. Maultzsch, P. Kim, L.E. Brus, T.F. Heinz, M. S. Hybertsen, G.W. Flynn, High-resolution scanning tunneling microscopy imaging of mesoscopic graphene sheets on an insulating surface, the, Proc. Natl. Acad. Sci. 104 (2007) 9209–9212.
[18] J. Sun, H.O. Finklea, Y. Liu, Characterization and electrolytic cleaning of poly (methyl methacrylate) residues on transferred chemical vapor deposited graphene, Nanotechnology 28 (2017) 125703.
[19] K. Hantanasirisakul, T. Chantaurai, A. Limsukhon, P. Chomkhuntod, P. Poprom, M. Sawangphruk, Size selection and size-dependent optoelectronic and electrochemical properties of 2D titanium carbide (Ti_3C_2Tx) MXene, Adv. Mater. Interfaces 9 (2022) 2201457.
[20] M.D. Montano, K. Liu, T. Sabo-Attwood, P.L. Ferguson, Analysis of single-walled carbon nanotubes in estuarine sediments by density gradient ultracentrifugation coupled to near-infrared fluorescence spectroscopy reveals disassociation of residual metal catalyst nanoparticles, Environ. Sci. Technol. 55 (2021) 1015–1023.
[21] V. Alzari, D. Nuvoli, S. Scognamillo, M. Piccinini, E. Gioffredi, G. Malucelli, S. Marceddu, M. Sechi, V. Sanna, A. Mariani, Graphene-containing thermoresponsive nanocomposite hydrogels of poly(N-isopropylacrylamide) prepared by frontal polymerization, J. Mater. Chem. 21 (2011) 8727.
[22] F. Bonaccorso, A. Lombardo, T. Hasan, Z. Sun, L. Colombo, A.C. Ferrari, Production and processing of graphene and 2d crystals, Mater. Today 15 (2012) 564–589.
[23] X. Sun, D. Luo, J. Liu, D.G. Evans, Monodisperse chemically modified graphene obtained by density gradient ultracentrifugal rate separation, ACS Nano 4 (2010) 3381–3389.
[24] W.J. Choi, Y.J. Chung, S. Park, C.S. Yang, Y.K. Lee, K.S. An, Y.S. Lee, J.O. Lee, A simple method for cleaning graphene surfaces with an electrostatic force, Adv. Mater. 26 (2014) 637–644.
[25] B. Cao, Y. Yuan, Z. Shan, Q. Wang, A. Abdelkader, A.R. Kamali, D. Montalvão, Effects of particle size on the separation efficiency in a rotary-drum eddy current separator, Powder Technol. 410 (2022) 117870.
[26] A.A. Nour, A. Abdelghani, R. Youcef, Simulation of eddy current separation of gold particles from sands, Int. J. Eng. Manuf. 6 (2016) 30–37.
[27] Z. Huang, J. Zhu, X. Wu, R. Qiu, Z. Xu, J. Ruan, Eddy current separation can be used in separation of non-ferrous particles from crushed waste printed circuit boards, J. Clean. Prod. 312 (2021) 127755.
[28] L.N. Pham, G.F. Tabor, A. Pourkand, J.L.B. Aman, T. Hermans, J.J. Abbott, Dexterous magnetic manipulation of conductive non-magnetic objects, Nat 598 (2021) 439–443.
[29] B. Guo, D. Li, J. Shi, Z. Gao, A performance prediction model for permanent magnet eddy-current couplings based on the air-gap magnetic field distribution, IEEE Trans. Magn. 58 (2022) 1–9.
[30] D.J. Efren, C.A. Cristina, A.S. Roberto, C.A. Eduardo, Modelling and test of an integrated magnetic spring-eddy current damper for space applications, Actuators 10 (2021) 1–18.
[31] Y. Yuan, B. Cao, X. Zhang, L. Feng, T. Wang, Q. Wang, Effects of material temperature on the separation efficiency in a rotary-drum type eddy current separator, Powder Technol. 404 (2022) 117449.
[32] C. Bin, Y. Yi, A. Abdelkader, A.R. Kamali, D. Montalvão, W. Qiang, S. Zhicheng, Y. Lixue, Generation mechanism and empirical model of eddy current force and torque in drum-type eddy current separation, Waste Manag. 182 (2024) 299–309.
[33] X.Y. Fang, X.X. Yu, H.M. Zheng, H.B. Jin, L. Wang, M.S. Cao, Temperature- and thickness-dependent electrical conductivity of few-layer graphene and graphene nanosheets, Phys. Lett. A 379 (2015) 2245–2251.
[34] D.O. Snyder, E.K. Koutsavdis, J.S.R. Anttonen, Transonic store separation using unstructured CFD with dynamic meshing, in: 33rd AIAA Fluid Dynamics Conference and ExhibitOrlando, Florida, 2003, p. 3919.
[35] B. Cao, Y. Yuan, Y. Arman, L. Feng, Z. Zhou, T. Wang, Q. Wang, Optimization of Halbach magnetic roller for eddy current separation based on the response surface method and multi-objective genetic algorithm, J. Clean. Prod. 278 (2021) 123531.
[36] C. Wang, Z. Hu, Q. Pang, L. Hua, Research on the classification algorithm and operation parameters optimization of the system for separating non-ferrous metals from end-of-life vehicles based on machine vision, Waste Manag. 100 (2019) 10–17.